Acta Materialia 199 (2020) 669–679

Contents lists available at ScienceDirect

Acta Materialia

journal homepage: www.elsevier.com/locate/actamat

Full length article

The isothermal evolution of nanoporous gold from the ring perspective - an application of graph theory

Markus Ziehmer[a,*], Erica T. Lilleodden[a,b]

[a] Helmholtz Zentrum Geesthacht HZG, Centre for Materials and Coastal Research, Institute of Materials Research, Materials Mechanics, Geesthacht 21502, Germany
[b] Hamburg University of Technology TUHH, Institute of Advanced Ceramics, Hamburg 21073, Germany

ARTICLE INFO

Article history:
Received 20 April 2020
Revised 6 August 2020
Accepted 10 August 2020
Available online 19 August 2020

ABSTRACT

The ring structures of five isothermally annealed nanoporous gold (npg) samples were analyzed explicitly by applying results and algorithms from graph theory to skeletonized 3D reconstructions from focused ion beam (FIB) tomography data. Simplified skeletons of the reconstructions were utilized, in which the real ligaments are reduced to straight edges between the branching points of the npg microstructure. So-called minimum weight cycle bases of each skeleton graph's cycle vector space were calculated, assigning different weight functions to these straight edges: equal weights, Euclidean lengths, and the real ligament lengths from backmapping the Euclidean skeleton edges to the skeletonized real ligament sections. These cycle bases contain the maximum number of linearly independent rings that cannot be generated by smaller rings via the ring sum specified in the cycle vector space. Such a decomposition of the npg network structures into the fundamental ring building blocks served to provide a new perspective of the isothermal evolution of npg, since the coarsening of the npg network structure could be examined from analyzing the local ring topologies and the classification of the ring topological classes. Our results suggest an increasing relative dominance of ligament pinch-off events over ring collapse events, manifesting in a broadening of the distribution of topological classes, and leading to a small but steady increase of the average number of ring edges. Furthermore, self-similar evolution of the investigated sample series cannot be stated. The implications on the topological evolution of npg as a function of the solid volume fraction are discussed.

1. Introduction

Nanoporous gold (npg) and other nanoporous materials have been the subject of many research activities in the past years, often due to the manifold application potential, but also in turn due to the fascinating microstructures that finally determine the behaviour in various ways, for an overview see [1]. After dealloying a precursor alloy, typically Ag_xAu_{1-x}, npg shows up as a three-dimensional ligament network, mostly described as a ligament-pore structure, that is bicontinuous over a certain range of precursor alloy composition x. It can be coarsened by annealing, thermodynamically driven by the reduction of interface area and associated excess energy. Such a coarsening results most visibly in an increase of the average ligament thickness. However, more appropriately, the network structure may be described as put together by torus-like rings, that are built up by ligaments interconnected across network branching points, rather than pores in terms of channel-like features.

Some practical importance of the rings has already been pointed out implicitly within the context of the micromechanical behaviour of npg [2,4,5], in terms of a *global* topological parameter [6], the overall connectivity C or genus g of the npg network structure. These two parameters are particularly well suited to characterize the global topology of porous network structures. However, it appears that they have been used in the literature on topological properties of microstructures more or less interchangeably and somewhat confusingly. Throughout this manuscript, we refer to the connectivity C as *the maximum number of cuts that can be made through a three-dimensional bulk feature before separating it into two non-connected parts*, as described in [6]. Fundamentally, topological properties are invariant under homomorphisms, i.e mappings that preserve such properties of a given space. One common and

* Corresponding author.
E-mail address: markus.ziehmer@hzg.de (M. Ziehmer).

https://doi.org/10.1016/j.actamat.2020.08.026

demonstrative example is the continuous deformation between a coffee mug and a donut (a torus), both having the connectivity $C = 1$. One can perform exactly one cut through the ring parts, the handle, of the two structures without cutting them into two separated pieces. Thus, a double-torus has connectivity $C = 2$, it has two handles or two rings. It is very important here to differentiate between three-dimensional, bulk features and two-dimensional surfaces. A simple example refers again to the connectivity C of a torus: it becomes one in the case of a bulk torus and two in the case of a "hollow", 2D surface torus. The confusion comes in part with the usage of the terms connectivity and genus. Basically, C or g are just one piece of the Euler characteristic χ, a topological invariant. This invariant is often being calculated from the number of surface mesh edges, faces and vertices that can be applied to three-dimensional features, e.g. [7]. There is a well known formula that relates χ and the genus g in such cases: $\chi = 2 - 2 \cdot g$. In [7], the authors use g as "a quantitative measure of the connectivity of a microstructure"'. There, g is the number of handles h minus the number of enclosed voids or cavities v. In this sense, this description appears to be in accordance with the treatment of χ in the case of three-dimensional structures using Betti numbers β_i, e.g. [8], where $\chi = \beta_0 - \beta_1 + \beta_2$. Here, the β_i relate to the number of connected components, the number of handles, and the number of cavities, respectively. The genus in [7] equals the difference $\beta_1 - \beta_2$ in [8]. These authors in turn denote β_1 alone as the connectivity. Thus, our C corresponds to h in [7] and β_1 in [8]. In [6], the authors do not take into account cavities, and describe the Euler characteristic as $\chi = N - C$, "the difference between the number of connected parts and the global connectivity of a feature set". Finally, to make connectivities of different samples comparable, one typically computes densities C_V, i.e. per unit sample volumes.

Actually, all what is known about the rings of npg network structures at this point bears on the analysis of one of these two, C or g, parameters. We employed computations of C using the open-source platform Fiji [9] and a plug-in therein, which is based on the theoretical treatment of voxelized data presented in [8]. It is worth mentioning that these authors claim to take into account the finite sizes of investigates volumes, i.e edge effects. The temporal evolution of the connectivity densities C_V of a npg sample series employed in [2,3], as-dealloyed and four samples isothermally annealed at a temperature $T = 300°C$ for different times and with solid volume fractions of ca. $30 - 32\%$, is shown in Fig. 1. There, annealing time $t = 0$ refers to the as-dealloyed state. One can see, that there is a drop of C_V, i.e. a reduction of the number of rings per unit volume, of three orders of magnitude over the total annealing time of 420min. Since no considerable densification effects or loss of the network interconnection could be detetected for this series, the mean ring sizes, characterized by the mean ring diameters $\langle D \rangle_{ring}$, increase with time, also shown in Fig. 1. Thus, annealing coarsens both the ligaments and the rings. Another important implication of these coarsening effects is a reduction of the number of ligaments (and nodes), because the interface area reduces and the ligament volumes increase with time. The oberservation that the number of rings decrease inversely with annealing time serves as a significant reminder of another network coarsening phenomenon, grain growth, where a grain boundary network undergoes topological transitions while reducing the number of grains. Consequently, the npg rings may be seen, equivalent to the grains in polycrystals, as the microstructural building blocks of npg.

Reanalyzing the isothermal coarsening process of npg from the perspective of *local* topologies appears to be inspiring, which results naturally from asking, which topological transitions are imaginable generally, and can lead to a net decrease in the number of rings over coarsening. In grain growth, typically three basic topological transitions are being described in the literature: neighbor switching, edge disappearance and grain disappearance events, e.g.

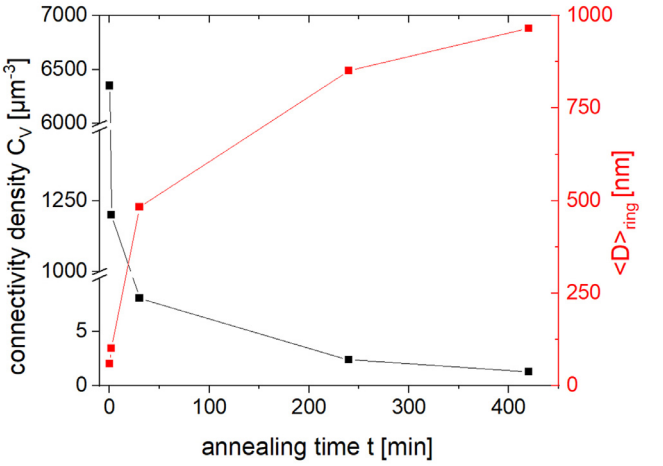

Fig. 1. The two plots shown in this figure highlight results from analyzing focused ion beam (FIB) tomography based 3D reconstructions of an isothermal npg annealing series of five samples, presented in [2,3]. The lines are guides-to-the-eyes. The plots summarize what is known at this point about the rings of the npg annealing series investigated. Annealing time $t = 0$ refers to the as-dealloyed state. The data in black shows the temporal drop of C_V, meaning that the number of rings reduces with time, see [2]. Please note the two-fold break of the y-axis! A consequence of this is an increase of the mean ring diameters, shown in red. These have been estimated in [3] to be roughly $2.3 \cdot \langle D \rangle_{lig}$, assuming the rings to be regular tori. (For interpretation of the references to colour in this figure legend, the reader is referred to the web version of this article.)

[11], the grains being characterized by their number of faces, edges and vertices. Naturally, the rings in npg would be characterized by their number of edges, i.e. ligaments connected via branching points, the nodes.

In npg, so-called ligament pinch-offs, singularities, described as solid-state Plateau Rayleigh instabilities [12], have been emphasized by various authors as one major ring reducing mechanism, see e.g. [10,13,14]. It seems there is no such equivalent described for topological transitions in grain growth. In [10], the authors also found from their MD simulations the reverse process, reattachments of pinched-off ligaments, which would be a ring creation process, that obviously has no equivalent in grain growth too. Additionally, they suggested another mechanism, which they called ring collapse, see Fig. 3 in [10]. While these authors describe this process as being driven by dislocation motion, we rather would refer to it as a result of a more fundamental topological transition that appears to be necessary during structural coarsening: a ligament disappearance transition, analogous to the edge disappearance events in grain growth. Above, we already mentioned the decreasing number of ligaments and nodes that is taking place upon coarsening. Here, we differentiate between such ligament reduction processes and the singular pinch-off events that also can effectively reduce the number of ligaments, as it is commonly believed that remnants from these events may flatten out upon further annealing. We think of processes that would locally lead to merging of ligaments and nodes, through the growing ligaments. We can think of different scenarios that eventually can also effectuate removal of rings, ring collapses, from the npg network, as explained below.

All these situations are sketched in Fig. 2 as simplified skeletonizations of the real situations. Real ligaments are represented by straight lines between red branching points, blue lines highlighting the specific edges that undergo a transition, and the neighboring edges in black. We use dashed lines, where we highlight the continuing network structure. In addition, to keep it general, we typically do not show closed rings with exactly specified numbers of edges, and thus describe relative changes of the number

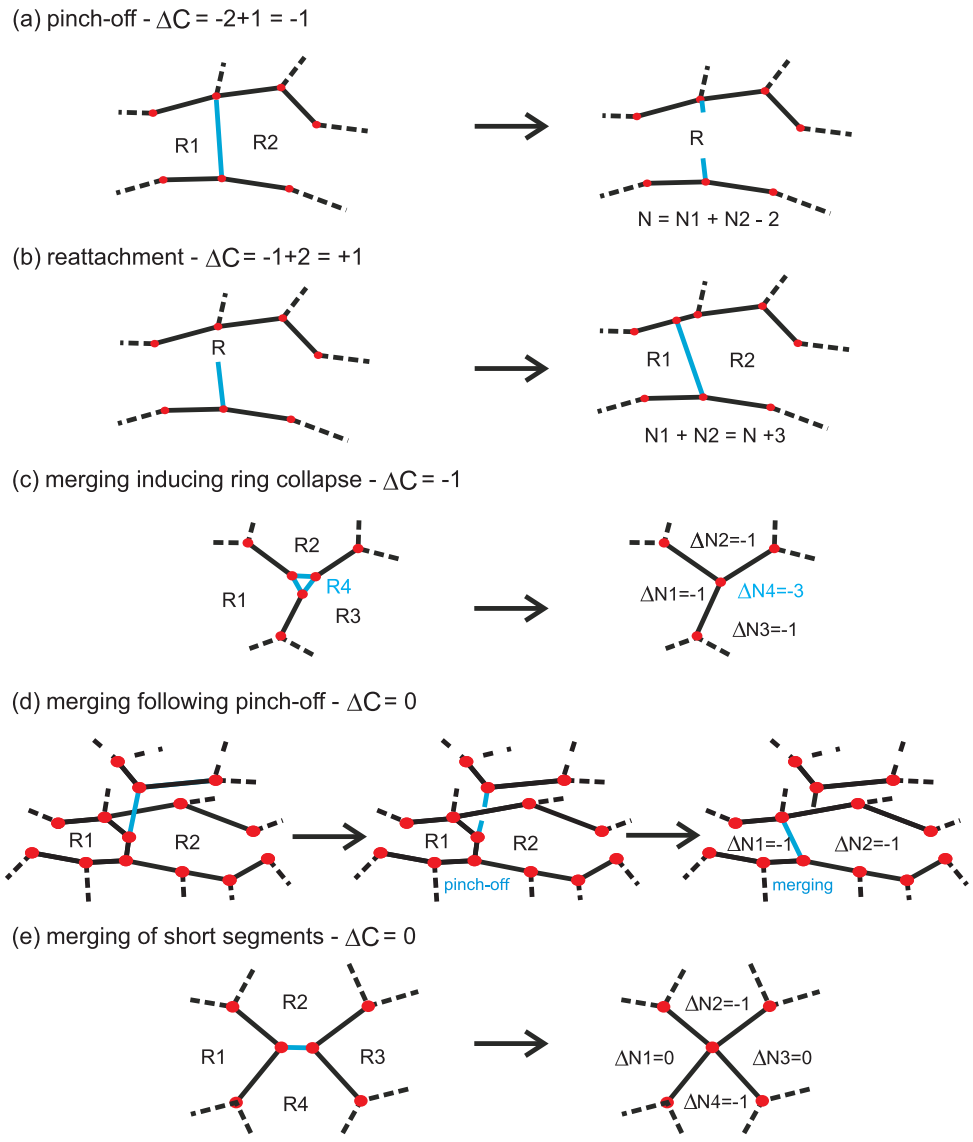

Fig. 2. Five sketches explaining basic topological processes that are imaginable in network structures like npg. In this skeletonized view, the ligaments are reduced to straight Euclidean connectors: solid blue the edges that undergo a transition and solid black the neighboring edges. Dashed edges indicate the continuing network. Branching points are shown in red In order to keep the description general, the rings are typically not closed, and consequently, relative changes of the number of edges ΔN and number of rings ΔC are given. For details, we refer to the text. (For interpretation of the references to colour in this figure legend, the reader is referred to the web version of this article.)

of edges of the involved rings, ΔN, as well as the relative change in the total number of rings, ΔC. In total, we describe five events, two of which reduce the number of rings, two keep it constant, and one would increase it. The situations typically employ nodes that are three-fold connected, but also four-fold connections may be generated. This relates to the fact that in npg of similar solid volume fraction, the structure consists mostly of these two types, as described in [15]. The two ring reduction events effectively reduce the number of rings, i.e the connectivity, by one, $\Delta C = -1$, but regarding local topology, they are fundamentally different. In the case of ring collapse, one ring is being removed from the system, in our view due to merging of edges. In Fig. 2(c), it is a (3-edged) ring $R4$, surrounded by the indicated neighboring rings $R1$ through $R3$, which disappears, *thereby reducing the number of edges of each neighbor ring* by one, $\Delta N_{1,2,3} = -1$. If existent, such processes would be mostly conceivable in cases, where the diameters of a ring's edges are much larger than the ring's hole is, and this does not need to be restricted to only 3-edged rings. It is very different in the case of ligament pinch-off due to the evolution of local curvatures and subsequently chemical potential. In Fig. 2(a), the blue ligament that is shared by the two rings $R1$ and $R2$, disconnects, and effectively $R1$ and $R2$ are removed from the system, while a new ring R is being created, having a *larger* number of edges, which is $N = N1 + N2 - 2$. In some sense, these pinch-offs resemble grain coalescence events following grain rotations [16], since two grains sharing one boundary are being combined to one single grain. Thus, in such a situation the change in connectivity is $\Delta C = -2 + 1 = -1$. Naturally, in a 3D interconnected, non-planar network, a ligament shared by more than two rings may disconnect, but this would also reduce the total number of rings effectively by one, e.g. three rings may be removed from the network while two new rings are being generated, both having larger numbers of edges. The inverse process, creation of two new rings by reattachment of a pinched-off dangling ligament would be described in the simplest case as the perfectly reverse act: remove a ring R with N edges, and create two new rings $R1$

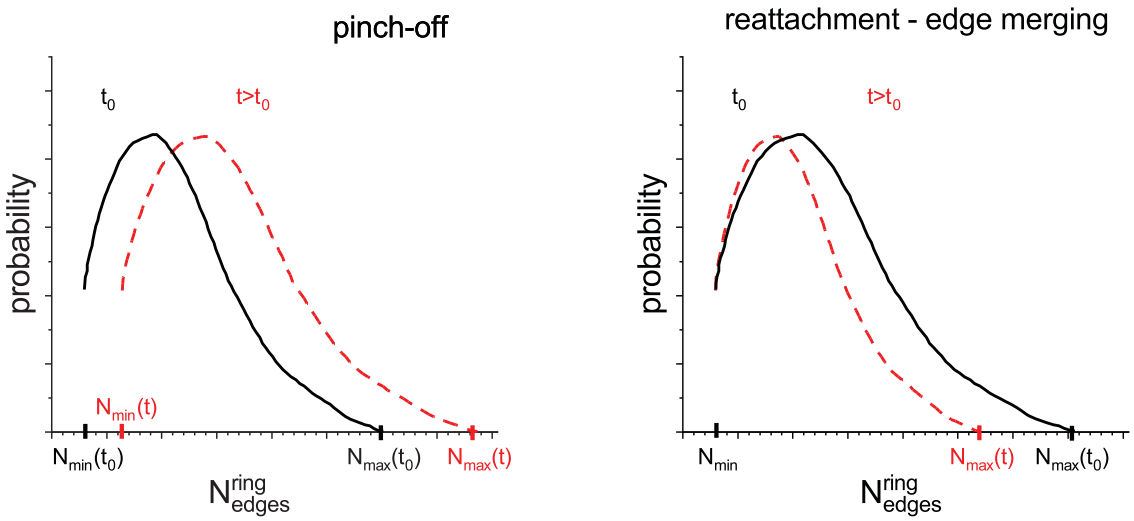

Fig. 3. The potential impacts of the various topological transitions on the discrete distribution of the number of ring edges over coarsening. We assume lognormal shape, simplified represented as a continuous distribution. In particular, the topological transitions described in the text can impact the domain of the number of ring edges in different ways, i.e. the interval $[N_{\min}, N_{\min}+1, \ldots, N_{\max}-1, N_{\max}]$ Examples at times t_0 and $t > t_0$ are indicated for each fundamental transition, see text for details. Altogether, depending on predominantly acting transitions or combinations, several scenarios are imaginable over coarsening: time-invariance, broadening or narrowing with a constant $N_{\min}$, with increasing $N_{\min}$, a shift, change of distribution type etc.

and $R2$, the number of edges $N1$ and $N2$ of which could be all combinations that would sum up to $N+2$. However, this would require reattachment of a dangling ligament to an already existent node. More probably, one would imagine creation of a new node, that could randomly take place anywhere in the structure. In any case, the change in connectivity in such a reattachment case would be $\Delta C = -1+2 = +1$, but the number of edges would follow the equation: $N1+N2 = N+3$, see Fig. 2 (b). In 2(d) and (e), we exemplify another two situations that would not change the number of rings, but only reduce the number of edges and nodes through merging events. We think that such topological transitions are fundamentally necessary processes of the structural evolution of npg. In 2 (d) we show the case that after pinch-off and smoothing of one pinch-off remnant, a situation may evolve that finally produces a node that would be two-fold connected. However, due to the ongoing growth of the ligament diameters, such a situation would effectively lead to a merging of this node into one single edge with a potentially much higher aspect ratio, and simultaneously reducing the total number of edges. Also, one could imagine that ligaments with low aspect rations are merged into one single larger node, shown in (e). Here, we do not claim completeness in the description of potential transitions. Instead, we are aiming at highlighting the importance of edge disappearance events, as we will explain in details below.

From these examples, it appears promising to decompose npg into its ring constituents, and characterize the rings by their number of edges. In other words, a npg network structure would be characterized by the topological classes of its rings, i.e. all rings with N edges belong to one class. This is in some way analog to what has been applied to polycrystalline materials, where the evolution of grain aggregates has been examined through the evolution of the grain boundary network topology, see e.g. the classical publications [17,18]. Thus, the coarsening of npg can be examined by following the evolution of such topological classes. In the case of the npg annealing series already published in [2,3], this reduces to following the evolution of discrete distributions of topological classes, due to the use of different sample volumes. So far, it is unclear how such distributions look in the case of npg. Besides a detailed topological characterization, an examination of the isothermal evolution of npg in this way helps to identify the dominant topological mechanisms at various stages. Also, it is still under debate, whether such high-genus systems can coarsen in a self-similar manner, or whether this is fundamentally impossible due to the pinch-off transitions that may act predominantly [13,14,19]. In particular, the analysis proposed here could be applied to systems exposing different solid volume fractions. There are indications that this parameter may critically act on the coarsening behaviour in various ways [13,19].

The basic events described above, pinch-off, reattachment and the edge reduction processes, act on the temporal evolution of the distributions in different ways, particularly with respect to the domains. This is highlighted in Fig. 3 in simple sketches, not taking into account details of the sizes of single classes. Here we assume a discrete distribution of the number of ring edges of a npg sample at a start time t_0, shown in black and for visualization purposes as a continuous distribution of lognormal shape. The domain of the distribution would range from topological class $N_{\min}$ to $N_{\max}$ in discrete unit steps, i.e. $N^{ring}_{edges} \in [N_{\min}, N_{\min}+1, \ldots, N_{\max}-1, N_{\max}]$. The edge reduction events can remove rings completely from the distribution through ring collapses, presumably from the lower indexed topological classes, and could in this way lead to an increase of $N_{\min}$ over time. However, as shown, *all* edge reduction transitions act on their neighbor rings by reducing the number of their egdes, which can affect rings of each topological class. This, will tranfer such rings into lower topological classes, and may thus keep $N_{\min}$ time-invariant and may also decrease $N_{\max}$. Ligament pinch-off events in turn convert rings of smaller number of edges into new higher-edged rings as explained, and thus statistically may increase $N_{\max}$ with time. These transitions alone could also lead to an increase of $N_{\min}$ through depletion of lowest indexed topological classes. Lastly, reattachments alone could, at least statistically, reduce $N_{\max}$ and also generate smallest rings, i.e. refill respective classes. Summarized, edge reduction processes, counteract pinch-off events with respect to the evolution of the distribution domains. This is also true for reattachments, but they also counteract on the global, temporal decrease of the connectivity, the number of rings. It should be kept in mind that all these transitions will affect the sizes of single topological classes, i.e. the number of rings populating a specific class. However, this cannot be detected from analyzing the sample series employed in this work. Overall, several scenarios are conceivable depending on predominant topological mechanisms or combinations: the distribution of topolog-

ical classes may be time-invariant, it may shift with or without broadening, $N_{\min}$ and $N_{\max}$ may change or not, or the type of the distribution may change.

To our knowledge, an attempt to analyze the npg ring structure explicitly has not been presented so far, even though the theoretical framework for extracting a network's ring or cycle content is given by graph theory [20–22]. "A simple graph G consists of a non-empty finite set $V(G)$ of elements called vertices (or nodes), and a finite set $E(G)$ of distinct unordered pairs of distinct elements of $V(G)$ called edges" [21]. This is essentially the situation that we encounter in npg: ligament sections (lines) that are connected by branching nodes (points), overall interconnected to one continuous component. Rings or cycles can be envisaged in the natural, intuitive way: a closed sequence of distinct points and lines. What may be potentially unknown even to persons who are familiar with the existence of graph theory is that in graph theory, a vector space description of a graph's cycle space has been developped, with all the features that we know from our standard Euclidean vector space, particularly vector space bases, that help finding solutions for specific cases [22,23], and that can be applied to decompose npg networks into their ring contents. In order to make graph calculations accessible to npg, skeletonized npg ligament networks appears to be best applicable. Skeletonization algorithms are available and can be applied to npg 3D reconstructions, such as the ones presented and examined in [2,3].

The ingredients for analyzing the npg ring structure are given, and their application to focused ion beam tomography (FIB) reconstructions of npg is presented. Section 2 provides a short mathematical description of the graph theoretical aspects used in this work, together with their application to the skeletonizations of FIB tomography npg reconstructions. Finally, in Section 3, the results achieved from the isothermal npg annealing series presented in [2] are shown and discussed with respect to their implications on the isothermal coarsening of the npg.

2. Graph theoretical aspects and their application to npg reconstruction skeletons

In this section we are not aiming at providing a comprehensive, mathematically puristic description of the graph theoretical aspects employed in this work, which is out of scope. Instead, we try to mathematically display the results from graph theory, as is necessary to follow and understand their application to our analysis. Otherwise, we refer the interested reader to various textbooks, e.g. [20,21,24]. While many aspects of graphs can be understood in a very intuitive approach, the translation into pure math language is not necessarily so.

In the work presented here, npg structures are modeled as simple, undirected and weighted graphs, without loops and multiple edges, i.e. rings have at least three edges. A graph is defined as a pair $G = (V, E)$ of sets with $E \subseteq [V]^2$. The elements of V are typically denoted as vertices v of G, elements of E are denoted as edges e of G, where in the case of undirected graphs, unordered pairs of vertices suffice to define the edges. We denote the number of edges m and the number of vertices n. The degree of a vertex is the number of edges incident to it. We define a weight function $w : E \to (0, \infty)$ that assigns strictly positive weights to the edges of E. The unweighted case relates to all edges having weight one, i.e. $w(e) = 1\ \forall e \in E$. A cycle Cy in a simple, undirected graph may be represented as a closed, natural and *ordered* sequence of distinct vertices $\{v_1, v_2, \ldots, v_{final} = v_1\}$, except that $v_1 = v_{final}$, or as a sequence of distinct edges. Fig. 4 gives a simple example of a graph, having one 3-, and some 4-, and 5-cycles, e.g. $Cy^3 = \{v_1 = v1, v_2 = v2, v_3 = v5, v_{final} = v1\} \widehat{=} \{e1, e5, e8\}$.

The cycles Cy of a graph G span a binary cycle vector space $\mathcal{C}(G)$ of G over the Galois field of two elements $GF(2)$. The dimension of $\mathcal{C}(G)$ is given by a graph invariant, the cyclomatic number $\mu(G) = m - n + c$, where c is the number of connected components in G. The cyclomatic number relates in fact to the Betti number β_1 described in the introduction, the connectivity C in this manuscript. These numbers become equal in the case that we remove all dangling edges from our structure, i.e. there would not be another ring built by edges inside *and* outside of the reconstruction box. With respect to the vector space description, this means that $\mu(G)$ gives the maximum number of linearly independent vectors of $\mathcal{C}(G)$ (as for vector space rules and properties, see math textbooks, e.g. [25]). The vectors in this space are the cycles, identified by edge-incidence vectors $(b_i(Cy))_{i=1,\ldots,m}$, i.e. the components are 0, if $e_i \notin Cy$ or 1, if $e_i \in Cy$. Thus, addition of two vectors $Cy_1 \oplus Cy_2$ is component-by-component according to the rules of the field $GF(2)$:

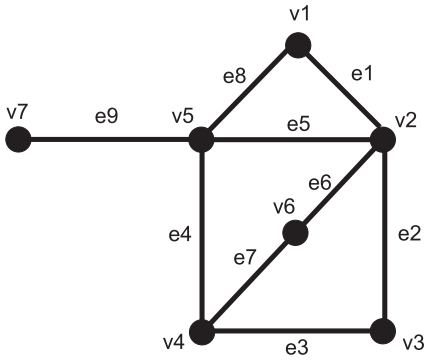

Fig. 4. A simple, one-component graph G is shown, with $V(G) = \{v1, v2, \ldots, v7\}$, i.e. $n = 7$, and $E(G) = \{e1, e2, \ldots, e9\}$, i.e. $m = 9$, with $e1 = \{v1, v2\}$ etc. One way, cycles can be referred to, is as natural and closed, i.e. $v_{initial} = v_{final}$, sequences of distinct vertices (except that $v_{initial} = v_{final}$), e.g. $\{v1, v2, v3, v4, v5, v1\}$, or as a closed sequence of edges, i.e. $\{e1, e2, e3, e4, e8\}$. Since we are dealing with simple graphs, the cycle lengths, i.e. the *number* of vertices or edges, is $|Cy| \geq 3$.

+	0	1	·	0	1
0	0	1	0	0	0
1	1	0	1	0	1

This corresponds to the symmetric difference $Cy_1 \oplus Cy_2 = (E(Cy_1) \cup E(Cy_2)) \setminus (E(Cy_1) \cap E(Cy_2))$, and effectively removes edges shared by the two non-disjunct cycles $Cy_{1,2}$. One example referring to Fig. 4 is: the 5-cycle $\{e1, e2, e3, e4, e8\}$ can be calculated as the sum of $\{e1, e5, e8\}$ and $\{e2, e3, e4, e5\}$. In the edge-incidence vector notation, this becomes:

$$Cy^3 = (1, 0, 0, 0, 1, 0, 0, 1, 0)$$
$$Cy^4 = (0, 1, 1, 1, 1, 0, 0, 0, 0)$$
$$Cy^5 = (1, 1, 1, 1, 0, 0, 0, 1, 0).$$

Component-by-component addition modulo 2 yields $Cy^5 = Cy^3 \oplus Cy^4$.

The weight of a cycle Cy is defined as $w(Cy) := \sum_{e \in Cy} w(e)$. The length of a cycle is its number of edges. A basis $\mathcal{B}(G)$ in the cycle space of G is a linearly independent set over $GF(2)$ of cardinality $\mu(G)$ of cycle incidence vectors. The weight of a basis $\mathcal{B}(G)$ is $w(\mathcal{B}) := \sum_{Cy \in \mathcal{B}} w(Cy)$. All cycles in a graph's cycle space can be generated by linear combinations of the cycle base vectors, according to vector space rules and the rules of the field $GF(2)$. There are various solutions to bases of this vector space, which are not unique in general [23]. So-called minimum weight cycle bases (MCB) appear most appropriate for many purposes [23,26]. MCB's are the largest linearly independent sets of cycles with minimum total weight; the largest set of cycles that cannot be generated by smaller cycles via the cycle space vector addition. Even though those are also not unique generally, the distribution of cy-

cle weights of all MCB's of a graph are identical, and an ordered weight vector can be defined, which is another graph invariant [23,27].

The cycle space dimension of the unweighted graph in Fig. 4 is $m - n + 1 = 9 - 7 + 1 = 3$, which is the maximum number of linearly independent rings, the "size" of a cycle basis of this graph, and the number of rings that seem to be naturally visible. For instance, one basis would be the two 5- and the single 3-ring:

$$Cy_1^5 = (1,0,0,1,0,1,1,1,0)$$
$$Cy_2^5 = (1,1,1,1,0,0,0,1,0)$$
$$Cy^3 = (1,0,0,0,1,0,0,1,0).$$

This basis would be of weight 13 in the unweighted case. However, there are three MCB, each of weight 11, in this graph, comprising Cy^3 and two of three 4-rings:

$$Cy_1^4 = (0,1,1,1,1,0,0,0,0)$$
$$Cy_2^4 = (0,0,0,1,1,1,1,0,0)$$
$$Cy_3^4 = (0,1,1,0,0,1,1,0,0).$$

One of the 4-rings is linearly dependent on the other two, which highlights the non-uniqueness of the MCB's of this graph, but the ordered weight vector would be of the form {3|4|4} in all cases.

Cycles that are elements of a MCB are called *relevant*. The graph in Fig. 4 has 4 relevant cycles from the union of all MCB's [26], i.e Cy is *relevant*: there are no cycles $Cy_1, \ldots, Cy_k$ with $Cy = Cy_1 \oplus \ldots \oplus Cy_k$ and $w(Cy_i) < w(Cy)$, $\forall i = 1, \ldots, k$. The intersection of all MCB's yields the set of *essential* cycles, which may be empty. In our example, the Cy^3 ring is essential. For further and more sophisticated information on MCB's and algorithms, see e.g. [22,26–29].

The FIB tomography reconstructions of an isothermal annealing series of npg, already utilized in [2,3], serve as the data base of our npg ring analysis. It consists of five samples, all generated from the same as-dealloyed master batch, that in turn was produced from a $Ag_{75}Au_{25}$ precursor alloy. This allows us to expect the initial structural conditions to be nearly identical. In particular, regarding the analyses presented in this manuscript, this relates to the initial number of rings per unit volume at time $t_0 = 0$, $C_V(t_0)$. One sample was left as-dealloyed and four samples were annealed at temperature $T = 300°C$ for different times $t = 2, 30, 240, 420$min. Finally, FIB tomography was done after epoxy-infiltrating these five samples in order to facilitate clean cross-sectioning. For each of the five samples, we could generate six reconstructions, which were believed to be of representative volume sizes, i.e. to reflect global properties of npg, see [2]. The annealing induced coarsening of the ligament sizes resulted in mean ligament diameters of ca. 26, 44, 210, 370 and 420nm, determined from the 3D reconstructions using the Fiji plug-in BoneJ [9]. This could be used to determine the growth exponent $n \approx 3.8$, indicative of surface diffusion driven coarsening. Also, already described above and shown in Fig. 1, the connectivity density values C_V were determined from the reconstructions. Details of the npg processing can be found in [30], and of FIB tomography and structural analyses in [2]. The npg microstructures of these reconstructions have been described as approximately statistically self-similar with respect to ligament diameters, connectivity, and morphology, even though there are indications that point to ongoing changes of scaled parameters during coarsening [2,3].

As mentioned above, skeletonizations of the reconstructions appear to be the natural starting point for an application of graph theory. In this study, we employed open-source 3D skeletonization algorithms within the Fiji software package [9]. In order to check the quality of the skeletons, we visualized the skeletons within semi-transparent isosurface representations of npg reconstructions. Fig. 5 highlights a subvolume from such a visualization. The branching points in the real structure seem to have been

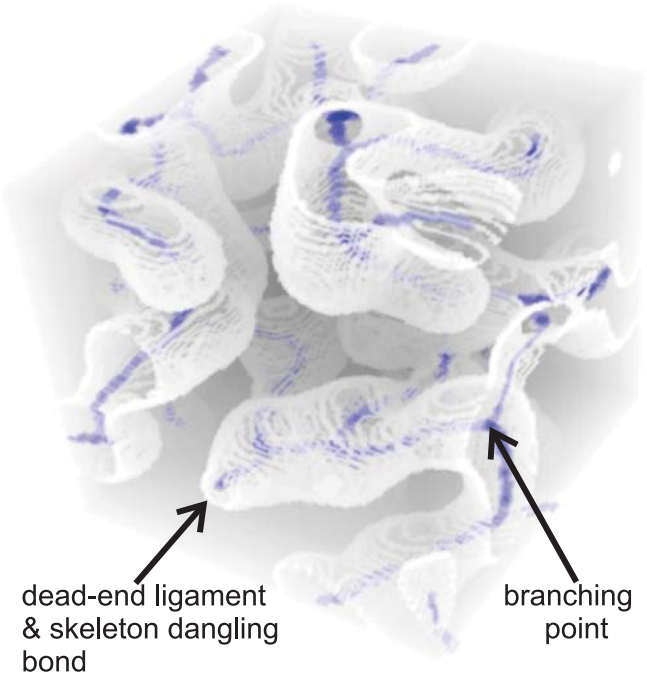

Fig. 5. A visualization highlighting the semi-transparent isosurface (white) of a npg reconstruction subvolume and its skeleton (blue). The skeletonization was performed in Fiji [9]. Indicated by the two arrows are examples of a branching point and a dead-end ligament, showing the good match of the skeletonization procedure. (For interpretation of the references to colour in this figure legend, the reader is referred to the web version of this article.)

matched very well. One example is indicated in the example. Also, it is well known that in npg, presumably from ligament pinch-off events, dead-end ligament sections can be found at all stages of coarsening. One of it can be seen in the low middle left of Fig. 5, also indicated, and it seems that these remnants are also mostly matched by the skeletonization procedure, appearing as "dangling bonds" in the skeletons. Dead-ends, or dangling edges, also result from the finite reconstruction volumes. Another very helpful feature of Fiji is the possibility of saving the skeleton data as either complete (as shown in Fig. 5) or reduced, i.e. as a set of connected node pair coordinates, either branching point pairs or branching point/dead-end point pairs. In the following, we also refer to this reduced skeleton as Euclidean skeleton, which is the structure we have calculated the npg ring content from. In a first step, all dangling edges were removed from the Euclidean skeleton, since they do not contribute to the rings, ending up with a skeleton having no vertices of degree one. This step introduced artificially vertices of degree two, like $v6$ in Fig. 4, which one should not have in such real structures. However, apart from the ones we generated in this first processing step, we also found such vertices throughout all our reconstructions, usually in very low quantities, i.e. ca. 1%, but even in much larger quantities for the five samples with $\langle D \rangle_{lig} \approx 370$nm. Due to streaks in the original SEM micrographs of this sample, that we relate to local charging due to the infiltrated epoxy, we applied a median filter to remove them. We finally found from backmapping the skeletonizations, the complete as well as the reduced, to the real structure, that the skeletonization of these reconstructions did not preserve the dangling bonds, also at the borders of the boxes, but identified correctly the branching points of the real structure. We are not sure whether this happened in response to the applied filter, or whether the skeletonization algorithm in Fiji was changed.

MCB's were then calculated, applying three different weight functions to the graph edges: equal weights (unweighted case), Eu-

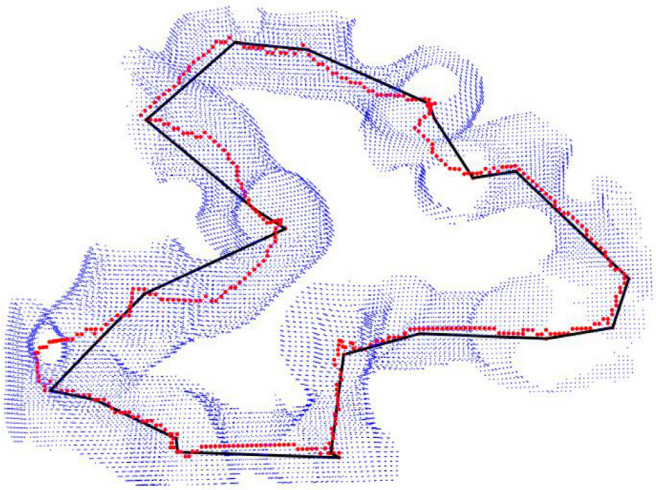

Fig. 6. An example of a detected ring, taken from the $\langle D \rangle_{lig} \approx 210$nm sample, exemplifying the backmapping from the Euclidean skeleton (black) over the complete skeleton (red) to the real structure (blue). Also, one qualitative finding of the ring analysis is the highly irregular shape of the rings. Particularly, rings can be spanned in three independent directions. Note that this cannot be represented appropriately here. (For interpretation of the references to colour in this figure legend, the reader is referred to the web version of this article.)

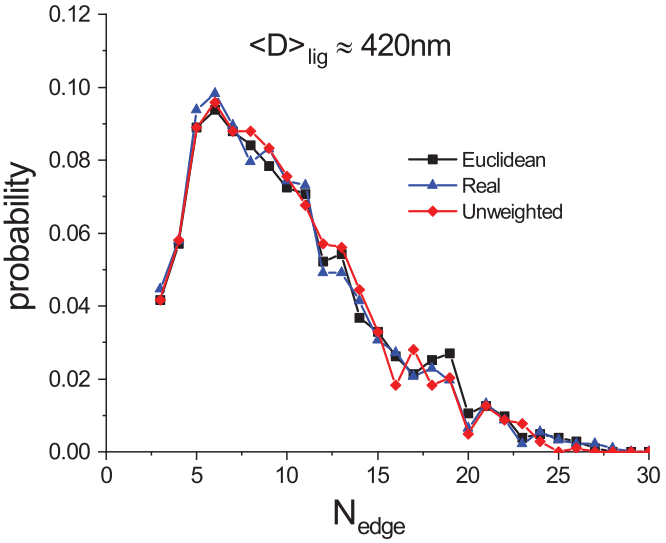

Fig. 7. The distributions of topological classes of the $\langle D \rangle_{lig} \approx 420$nm sample, resulting from the three different weights applied to the graph edges, and exemplifying that the distributions are essentially independent from these, which is the case for the entire sample series.

clidean edge lengths and "true" ligament lengths from backmapping. Differently weighted graphs will have some effect on the details of MCB's, since it is not expected that the ratio of true ligament length to Euclidean length is constant, nor that the ligaments are of equal length. Depending on the specific physical situation, this can become important. Here, we want to check whether it makes a difference topologically.

Fundamentally, the analyses presented in this work rely on the reconstructions. It should be noted, that particularly the two samples with the smallest structural sizes, i.e. $\langle D \rangle_{lig} \approx 26$ and 44nm, definetely pushed the limits of the FIB tomography approach, as we already mentioned in our previous publications. Also, SEM secondary electron imaging of a npg/epoxy surface is not a perfect surface representation due to electron penetration depths in epoxy, even at the low voltages of 2kV that we used, and the post-processing needed to achieve the reconstructions may act in some unknown way on the results. Most naturally, one may imagine loss of thinnest ligaments or ligament sections. This would result in an underestimation of the number of rings, as well as potentially overestimate $N_{\max}$ of the distributions. Also, the ligament network volume fraction may be overestimated locally, which may even lead to artificial interconnections, i.e. rings. Naturally, all this may sensitively act on the skeletonizations, but it is out of scope to reasonably quantify such potential artifacts. On the other hand, all our structural analyses performed so far, appear to be very consistent and reasonable. Additionally, through the backmapping, we are able to show the rings that we extract from our analysis.

In total we could analyze 1923, 1858, 192, 1420, and 1034 rings from the annealing series, given in order of annealing time. The sample that has been annealed for 30min has always been the outlier in our various analyses, see [2,3], and from the rather bad statistics here with only 192 rings, we conclude that the reconstructions had become too small regarding the question of representative volumes, see [2]. Nonetheless, it should at least serve as a good random sample.

Exemplarily, Fig. 6 presents a ring having 22 edges, highlighting the complete backmapping, the Euclidean edges in black, the complete skeletonized ligament sections as red points, and the real structure as a semi-transparent isosurface in blue. This example qualitatively shows that the npg rings are highly irregular shaped tori, particularly the larger ones.

3. Results and discussion

In Fig. 7, we exemplify with the $\langle D \rangle_{lig} \approx 420$nm sample results that the different edge weights applied do not have a major impact on the distribution of ring topological classes, the lines being guides-to-the-eye. The same holds for the rest of the annealing series. Of course, the sets of MCB deviate to some extent with respect to the specific rings, since the algorithm used for finding a MCB includes a search for shortest paths between vertices. These paths can vary depending on the ratios between true ligament length, Euclidean length and weight one of specific ligaments.

Fig. 8 top shows the results from the entire annealing series. Since the distribution of the 2min anneal looks very similar to the as-dealloyed one, and the distribution of the 240min very similar to the 420min anneal, we remove these two for clarity, see Fig. 8 bottom. The basic observations are: there is a significant probability larger than zero of finding rings with only three edges over the entire temporal evolution of the sample series, $P\left(N_{edge} = 3\right) > 0$, and the maximum number of ring edges $N_{\max}$ increases with time. This together leads to a broadening of the distributions of ring topological classes with time. The distribution from the 30min anneal, having the worse statistics, although appearing a bit spiky, presumably due to the worse statistics, may indicate the transition between the earliest and the later stages of evolution of this sample series.

At first, we conclude, or at least speculate, from these observations that pinch-off transitions are not the only operative mechanism, since otherwise, statistically, one may have expected a depletion of the lowest indexed classes, and possibly an increase of $N_{\min}$, see Fig. 3. Regardless of the overall broadening of the distributions, the as-dealloyed distribution of topological classes and the one after the first annealing step are essentially time-invariant, which is also the case for the two samples in the later coarsening stage, see Fig. 8 top. Given the very different dynamics in the earliest and late stages, this may appear somewhat surprising. Here, with dynamics we mean the time needed to induce relative changes of a structural parameter, in particular the dynamics of the reduction of the number of rings. This can be inferred from

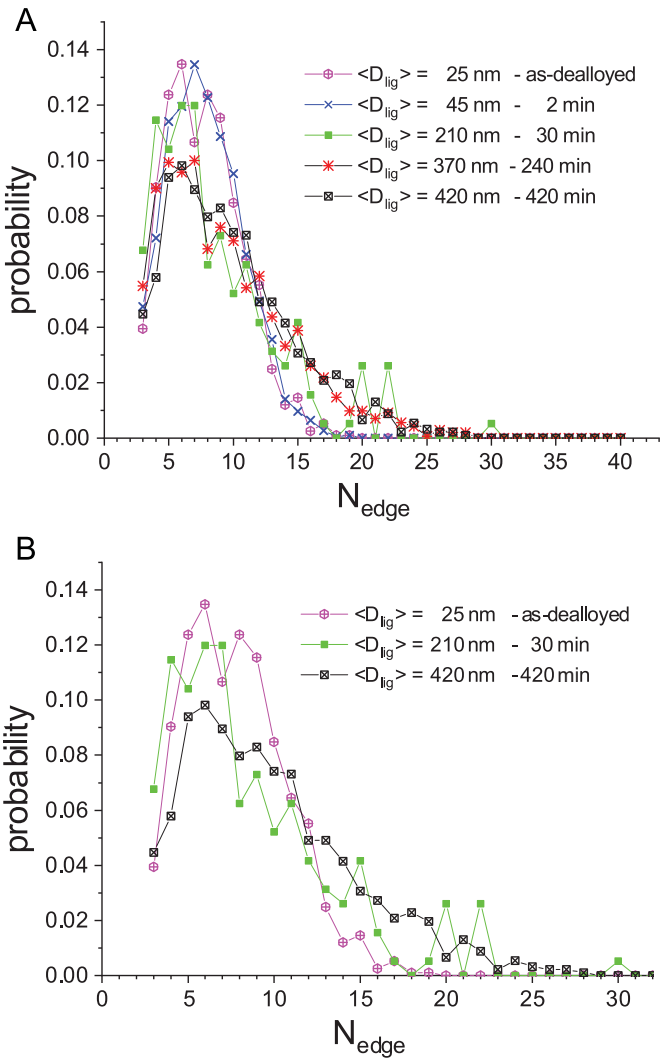

Fig. 8. Top: The distributions of topological classes from all five samples of the annealing series. Bottom: For clarity of presentation, the distributions of the $\langle D\rangle_{lig} \approx 44$nm and the $\langle D\rangle_{lig} \approx 370$nm sample are removed here, since they are very similar to the results from the as-dealloyed and the longest annealed samples. Clearly, the main observations are: $P(N_{edges} = 3) > 0$ at all times; $N_{\max}$ increases with time. This together leads to a broadening of the distribution of the number of ring edges with time.

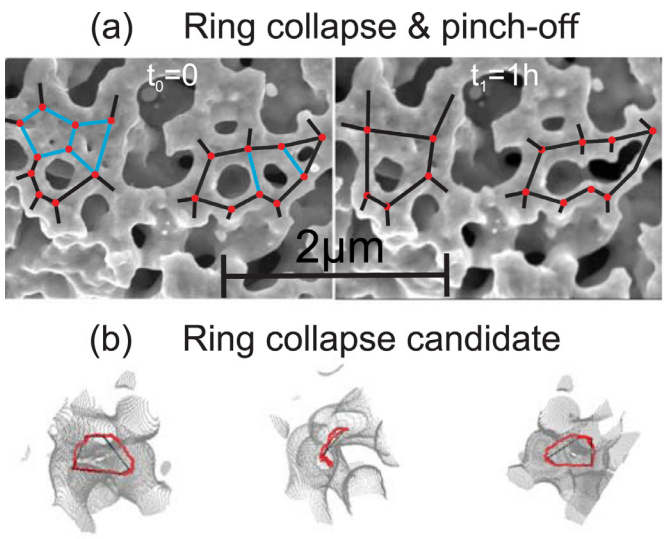

Fig. 9. (a) SEM micrographs demonstrating ring collapse and pinch-off events that happened during annealing at a temperature $T = 350^{\circ}$C in an npg sample of about 30% solid volume fraction. A 4-edged and a 5-edged ring exposing very small holes with a diameter of ca. 40nm and edges with diameters between ca. 150 and 600nm collapsed during the annealing step. On the right, two pinch-off events happened during the annealing step of 1h. Finally, three rings were converted into one new, larger ring. (b) A 5-edged ring rollapse candidate extracted from one latest stage reconstruction with $\langle D\rangle_{lig} \approx 420$nm. Three perspectives are shown for clarity, as well as the Euclidean and the real skeleton.

Fig. 1, where it can be seen that it is $C_V^{-1} \propto t$, i.e. $C_V^{-1}(t) = A \cdot t + B$. Here, B denotes $C_V^{-1}(t_0)$, the inverse number of ring density of the as-dealloyed state at time $t_0 = 0$. This can be used to estimate for example the time needed to cut in half the number of rings. For $C_V^{-1}(t) >> C_V^{-1}(t_0)$, it follows $t_2 = 2 \cdot t_1$, both times being related to the same reference time, which means that one needs to double consecutive annealing time steps. For the annealing series employed here, we find a relative drop of the connectivity density C_V of about 80% in the first two annealing minutes, and of about 40% in the last annealing step of 180min.

The fact that there is no significant evolution of the distribution during the first annealing step, i.e. a change in $N_{\min}$ or $N_{\max}$ or a change in distribution type, may be interpreted in two ways. As described in Section 2, the structures of the two earliest stages, as-dealloyed and first annealing step, pushed the FIB tomography. It may be particularly the reconstruction of the as-dealloyed state that overestimates $N_{\max}$, as described, and we may have simply not resolved the already ongoing distribution broadening, induced by predominantly acting pinch-offs. On the other hand, overestimation of $N_{\max}$ could be true likewise for the first annealing step sample. This error is difficult to estimate, and we would like to give another interpretation, accepting the early stage results as is. If only one of the proposed mechanisms were predominant, this would have involved a change in the distribution of topological classes. If we may believe in pinch-offs to occur at all times, then balancing the effects of these transitions onto the evolution of the distribution of topological classes must have happened under the constraint of a large drop of C_V in these first two minutes, see Fig. 1. We cannot exclude reattachment events, but these would counteract on the reduction of C_V. Also, to our knowledge, there is no experimental verification for such events so far. However, we think we have strong indications for the existence of ring collapses. In Fig. 9, we show results from an non-isothermal annealing experiment on npg of nominally same solid volume fraction, performed at a higher temperature $T = 350^{\circ}$C. Two ring collapse events and also two pinch-offs are highlighted, that happened during later coarsening stages. The two ring collapses exemplify the situation that we proposed in the introduction, merging of rings with small holes compared to ligament thicknesses. We also found examples of such rings from late stage reconstructions, one of which we show here. Visualizations of rings from early stage reconstructions are less demonstrative due to the worse resolution, i.e. ratio of mean ligament thickness to voxel sizes. The existence of ring collapses can explain the existence of 3-edged rings throughout the entire annealing series. We think, it is conceivable that in general edge reduction processes are operative. Altogether, we conclude that in the beginning of coarsening all mechanisms were available and balanced, and a transformation of such availability of mechanisms during structural coarsening took place. This is indicated by the broadening of the distribution due to a seemingly increasing, relative dominance of pinch-off events, since only these topological events can statistically increase $N_{\max}$, as described above.

To further understand this, we performed a detailed statistical analysis of the ring sizes and the evolution of averages along the five points in time specified in the annealing series, which became accessible through the backmapping from the reduced, Euclidean

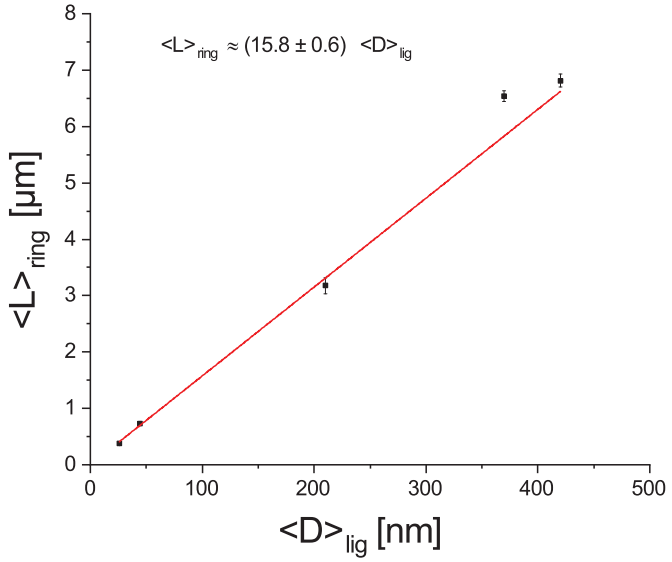

Fig. 10. The mean ring size $\langle L\rangle_{ring}$, analyzed as the line circumference of the ring skeletons, scales linearly with the respective mean ligament diameters $\langle D\rangle_{lig}$ by a factor of ca. 16. As a result, also the average growth rate of the ring circumference is 16 times larger than the average growth rate of the ligament diameters, see text for details.

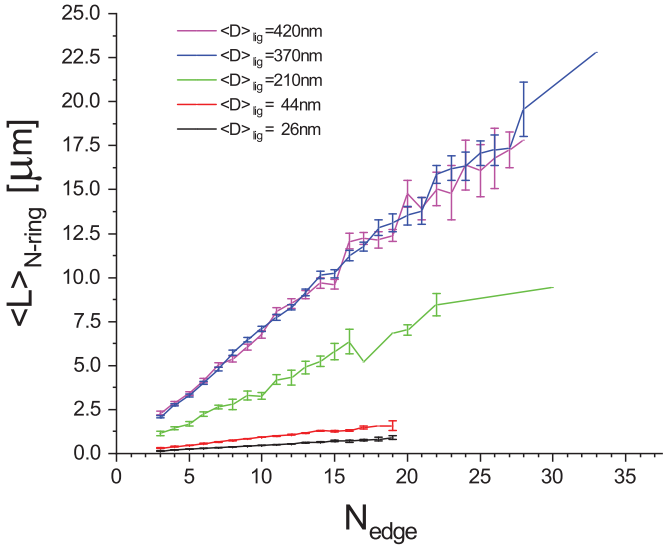

Fig. 11. The mean ring sizes of the topological classes N for the five samples, $\langle L\rangle_{N-ring}$ scale linearly with the number of ring edges N_{edge}. The increasing slopes reflect the increasing mean ligament lengths $\langle L\rangle_{lig}$. It can be seen that $\langle L\rangle_{N-ring}$ essentially grows with time for all topological classes N_{edge}. In the late coarsening stage, the difference between the last two samples are marginal.

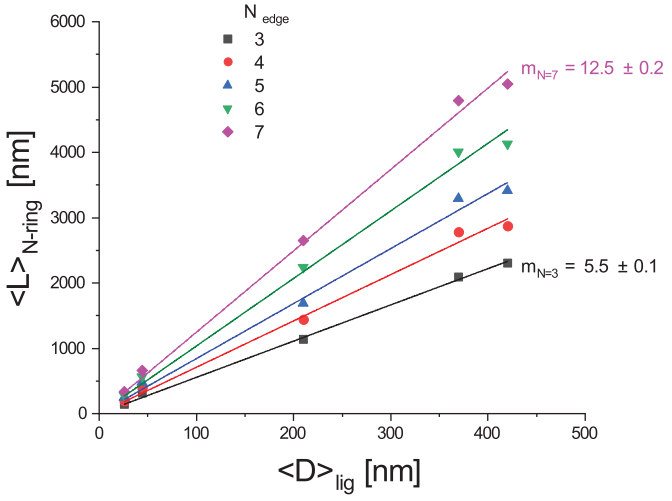

Fig. 12. The mean ring sizes of the topological classes $N = 3$ to 7 scale linearly with the mean ligament diameters $\langle D\rangle_{lig}$, cmp. to Fig. 10. The slope m, explicitly shown for $N = 3$ and 7, scales with N. It can finally be shown that the average ring growth rates for all N are larger than the average ligament diameter growth rate, see text. From this, we deduce that the probability of ring collapses strongly decline over time.

ligaments to the completely skeletonized ligaments, see Fig. 6. The ring sizes can then be described and approximated by the total line length of those skeleton sections that build a specific ring, i.e the ring sizes are described by line circumferences, in Fig. 6 the line that would pass through the red dots. In particular, we can connect the single ring sizes with the topological classes they are belonging to. Even though, our dataset does not allow to identify the temporal evolution of single rings, the approach can help to illustrate decisive factors.

In Fig. 10 the mean ring circumference $\langle L\rangle_{ring}$ is plotted against the mean ligament diameter $\langle D\rangle_{lig}$. It is seen that there is linear relationship between the two structural parameters, with a slope of about 16, which in particular means that the growth rate of the average ring sizes, as determined via the average circumferences, is 16 times higher than for the average ligament diameters, i.e. $\Delta\langle L\rangle_{ring}/\Delta t \approx 16 \cdot \Delta\langle D\rangle_{lig}/\Delta t$. This approach can be further refined by application to the single topological classes. In Fig. 11, the mean ring sizes of the single topological classes $\langle L\rangle_{N-ring}$ are shown for all five samples as indicated. It can be seen that for each sample $\langle L\rangle_{N-ring}$ goes linearly with the number of edges referred to the topological class, i.e $\langle L\rangle_{N-ring} \propto N_{edge}$, and the slope increases with $\langle D\rangle_{lig}$. This increasing slope m simply reflects the average ligament length $\langle L\rangle_{lig} \approx m = \Delta\langle L\rangle_{N-ring}/\Delta N_{edge}$, that's increasing over coarsening of the structure. Secondly, during annealing, $\langle L\rangle_{N-ring}$ is growing for *all* N_{edge}. This is highlighted in Fig. 12, where the dependency of $\langle L\rangle_{N-ring}$ from $\langle D\rangle_{lig}$ is shown for the first five N_{edge}-classes. There is a linear relationship for all classes with an increasing slope m_N, which means that the growth of the average ring size of a specific topological class depends on the number of ring edges defined by this class. At a first glance this may appear surprising, but the reason simply is, that the mean ligament *length* $\langle L\rangle_{lig}$ increases with time.

If we now apply a simplified geometrical model to the rings, treating them as regular tori, i.e. circles in a skeletonization, we may calculate the average ring diameter of each topological class as $\langle D\rangle_{N-ring} = \langle L\rangle_{N-ring}/\pi$, and thus $\Delta\langle D\rangle_{N-ring}/\Delta t = \Delta\langle L\rangle_{N-ring}/\pi\,\Delta t$. From Fig. 12 we see that $m_N = \Delta\langle L\rangle_{N-ring}/\Delta\langle D\rangle_{lig}$, and finally altogether:

$$\Delta\langle D\rangle_{N-ring}/\Delta t = \Delta\langle L\rangle_{N-ring}/(\pi\,\Delta t) = \left(\Delta\langle D\rangle_{lig}/\Delta t\right)\cdot(m_N/\pi)$$

at all times and for all topological classes, or expressed slightly different:

$$\Delta\langle D\rangle_{N-ring}/\Delta\langle D\rangle_{lig} = m_N/\pi > 1,$$

since $m_N \geq 5.5$. As a consequence, the condition for ring collapse more and more worsens over annealing, because the average distances between ligaments to be covered to close a ring, whatever process is acting in details, become larger and larger, and the average ring diameters grow faster than the average ligament diameters, no matter which topological class.

We want to emphasize again that this explanation describes the evolution of *average* values, and additionally the ring shapes are considered regular tori, which they typically are not, see Fig. 6. Nonetheless, it may describe the underlying phenomena. Also, the data set employed here does not allow for checking the interfacial evolution, ring growth or topological transitions locally. This

requires a single volume data set with a sufficient time resolution compared to interface evolution speed, and sufficient size in order to statistically significant track the growing ring sizes. This is achievable at least for mid-stage coarsening regimes. In reality, due to the complex morphologies, local evolution imposes an intricate issue, see [31,32], but transitions between topological classes would be observable and help understanding the details.

Now, we discuss the conditions for pinch-offs to occur over annealing. Solid state Rayleigh-instability pinch-offs of solid cylindrical rods have been typically described as being driven by capillarity-induced surface diffusion, and a critical perturbation wavelength λ_{crit} of radial fluctuations to grow has been stated to be larger than $2\pi \cdot R_0$, or in a different analytical approach larger than $9/2 \cdot R_0$, R_0 being the initial radius of the cylinder, e.g. [12,33,34]. We may transfer this analysis to npg as an approximation, from which follows that the ligament aspect ratios may serve as a critical parameter, i.e. $\lambda_{crit} \approx L_{lig}^{\min} > 9/2 \cdot R_0 = 9/4 \cdot D_0 \approx 9/4 \cdot \langle D \rangle_{lig}$. Normalizing the analyzed ligament lengths L_{lig} by the respective mean ligament diameters $\langle D \rangle_{lig}$ and calculating the quantitites of ligaments the aspect ratios $L_{lig}/\langle D \rangle_{lig}$ of which are larger than 9/4 yields values between 31% and 44% (ca. 37, 44, 35, 38 and 31% in the order of annealing times), oscillating around a mean value of 37%. Thus, the aspect ratios serve as a descriptor of pinch-off probability, and as a rough estimate of the evolution of pinch-off conditions.

In total, we conclude that the probability for ring collapse strongly drops over time, while the probability for pinch-offs remain roughly constant. Overall, effectively this results in an increasing relative dominance of pinch-off events that manifests in the broadening of the distributions of topological classes, see Fig. 8.

In the late stages, the dynamics have slowed down considerably. Nonetheless, there's a significant reduction of C_V during the last annealing step, but no significant change of the distribution, particularly no further notable increase in $N_{\max}$. The discussion before implied ring collapse events to becoming unlikely at this stage of coarsening, although not necessarily impossible, see Fig. 9, and considering the highly irregular ring shapes one may even think of partial ring collapses. Instead, ring reduction is expected to be completed mostly by pinch-offs, increasing by chance $N_{\max}$. Considering the number of rings detected for the last sample, statistically we should have detected an increase of $N_{\max}$, but we cannot exclude without fail having potentially missed necessary very large rings due to the finite reconstruction volumes. Otherwise, assuming the distribution does represent the "true" distribution at this stage, then pinch-offs that have reduced the number of rings may accidentally not have lead to rings that would have increased $N_{\max}$. As described above, pinch-offs generates rings with an edge number according to $N_{new} = N_{ring_1} + N_{ring_2} - 2 \cdot N_{shared-edges}$, i.e. the generation of new appropriate rings requires pinch-offs to happen at the right places.

What are the implications of these results and the interpretation given on the coarsening behaviour of npg and other metallic nanoporous systems? Apart from application-oriented topics, the question of self-similarity has always been a subject of interest, see e.g. [2,3,13,14,19,35].

Regarding the system investigated here, self-similarity cannot be confirmed for the topological evolution of the annealing series in total. This appears to be consistent with various results already published by the authors, in particular the ligament size evolution [2], as well as the morphological evolution [3]. In [2], the authors stated the system to be sufficently or approximately self-similar with respect to the micromechanical aspects examined. Nonetheless, despite the just small differences, the scaled ligament distributions showed some evolution. Likewise the scaled interface shape distributions (ISD), investigated in [3] exhibited some evolution, see Fig. 5 therein. Similar to the local topology evolution, the scaled ISD appear to show two distinct stages of evolution, the ISDs from the first two samples being similar, as well as the two late stage ISDs, and some transition in between. It is particularly the range of the principal curvature value, κ_1 there, that the authors propose to reflect the rings, that appears to broaden a bit over time. From the results presented in this manuscript, we may assign this to the broadening of the distributions of topological classes, and consequently, this should be also reflected in the scaled ring length distributions. These are shown in Fig. 13, and indeed can a transition to larger scaled ring circumferences be seen there, that relates to the increase of the maximum number of ring edges $N_{\max}$ with time. The late stage results of this annealing series may be interpreted in a way that the system may have reached a steady state regime. However, if the pinch-offs do finally dominate the topological evolution, then self-similarity is not achievable fundamentally.

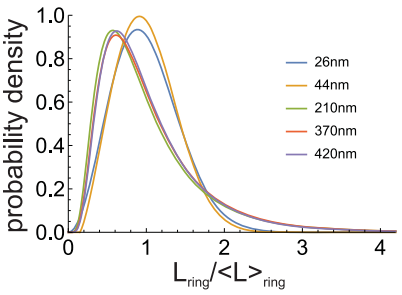

Fig. 13. Scaled ring line circumference distributions. This result is in line with the evolution of the distribution of topological classes, see Fig 8. The increase of $N_{\max}$ during coarsening also leads to an increase of the size of the largest rings, expressed in this plot as an increase in the ring size domain of the late stage samples.

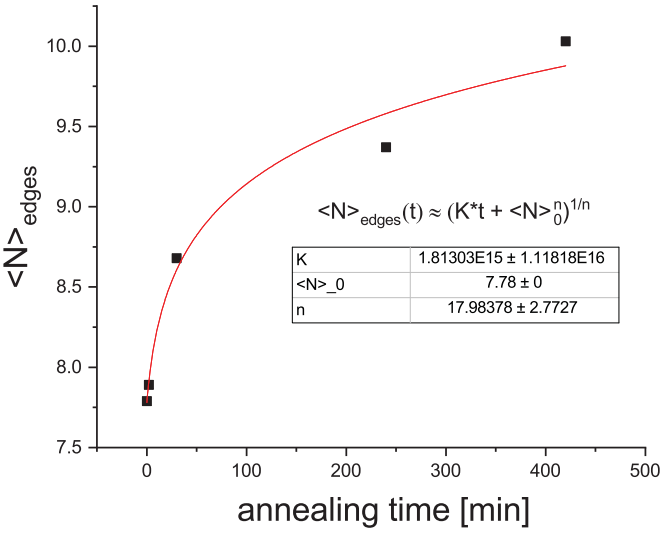

Fig. 14. The broadening of the topological distributions with time results in an steady increase of the average number of edges of a ring. The results can be fitted with a standard growth equation as shown. The result suggest that for very long times, values of $\langle N \rangle_{edges} \approx 13 - 14$ would be reached.

The broadening of the distributions of topological classes with time should impact the average number of ring edges $\langle N \rangle_{edges}$, and it turns out that this parameter scales linearly with $\langle D \rangle_{lig}$, not shown here. The temporal evolution is shown in Fig. 14. Even though the rate of increase of $\langle N \rangle_{edges}$ is small, the trend is unequivocal within the total annealing time applied in this study. We can fit a general growth equation to the data as shown. The result implies that for very long times, the system may reach values of $\langle N \rangle_{edges}$ of around 13 to 14.

The discussion above about the different topological events acting and their importance at different stages of structural coarsening implies that changing the initial conditions, i.e. the as-dealloyed topological state, may impact the relative weights of the different mechanisms in the early coarsening stages, and thus the ongoing topological evolution and related structural values. Apart from detailed dealloying procedures and conditions, the solid volume fraction ρ_{solid} can be expected to distinctly alter such initial topological states, because this parameter goes directly into the connectivity density C_V (or likewise the genus density), see e.g. [36]. Increasing ρ_{solid} increases C_V, the number of rings per unit volume, which should change the distribution of topological classes along with the ring sizes towards higher fractions of rings having lower numbers of edges. If our discussion and interpretations above prove to be well-founded, this may increase the relative weight of ring collapse events, and also pinch-off conditions, with corresponding consequences on the ongoing coarsening process. Simulation work on bicontinuous structures strongly suggests a major impact of these parameters on the ability of such systems to reach a self-similar state or not, e.g. [13].

Finally, understanding the details of the topological restructuring processes required observing transitions between topological classes, instead of overall transitions between distributions of topological classes, i.e. particularly a much better time-resolution than what has been achieved with the sample series investigated here. Achieving this experimentally appears to be very hard if not impossible at least for the earliest stages, but doable computationally.

4. Summary

In this manuscript, we presented an analysis of the local topological states of isothermally coarsened npg structures. Application of concepts and results from graph theory enabled the distributions of topological classes to be extracted from skeletonizations of 3D reconstructions, i.e the structures were characterized by the number of ring edges. One major result is a transition between the earliest and late stages of structural evolution that potentially implies a change of the relative weight of the predominantly acting mechanisms that reduce the number of rings over coarsening. As a consequence, self-similar evolution cannot be stated for the system inverstigated. The analysis given here suggests a promising approach to better understand the details of structural coarsening as a function of solid volume fraction of such bicontinuous systems, since the results and their discussion imply that the initial local topological state mostly impacts the relative weights of the ring reducing mechanisms, which in turn determines the ongoing structural evolution.

Declaration of Competing Interest

The authors declare that they have no known competing financial interests or personal relationships that could have appeared to influence the work reported in this paper.

The authors declare the following financial interests/personal relationships which may be considered as potential competing interests.

Acknowledgement

Funded by the Deutsche Forschungsgemeinschaft (DFG, German Research Foundation) - Projektnummer 192346071 - SFB 986. The authors thank Kaixiong Hu, currently at Wuhan University of Technology, for the reconstruction data.

References

[1] J. Weissmüller, K. Sieradzki (Eds.), MRSBulletin-Dealloyed Nanoporous materials with interface-controlled behavior, 43 (1), Cambridge University Press, Cambridge, 2018.
[2] K. Hu, M. Ziehmer, K. Wang, E. Lilleodden, Nanoporous gold: 3D structural analyses of RVEs and their implications on scaling relations of mechanical behavior, Philos. Mag. 96 (32–34) (2016) 3322–3335.
[3] M. Ziehmer, K. Hu, K. Wang, E. Lilleodden, A principle curvatures analysis of the isothermal evolution of nanoporous gold: quantifying the characteristic length-scales, Acta Mater. 120 (2016) 24–31.
[4] L. Liu, X. Ye, H. Jin, Interpreting anomalous low-strength and low-stiffness of nanoporous gold: quantification of network connectivity, Acta Mater. 118 (2016) 77–87.
[5] N. Huber, Connections between topology and macroscopic mechanical properties of three-dimensional open-pore materials, Front. Mater. 5 (2018) 69.
[6] J. Russ, R. DeHoff, Practical sterology, Springer, New York, 2000.
[7] R. Mendoza, K. Thornton, I. Savin, P. Voorhees, The evolution of interfacial topology during coarsening, Acta Mater. 54 (2006) 743–750.
[8] A. Odgaard, H. Gundersen, Quantification of connectivity in cancellous bone, with special emphasis on 3-D reconstructions, Bone 14 (1993) 173–182.
[9] J. Schindelin, I. Arganda-Carreras, E. Frise, V. Kaynig, M. Longair, T. Pietzsch, S. Preibisch, C. Rueden, S. Saalfeld, B. Schmid, J.-Y. Tinevez, D. White, V. Hartenstein, K. Eliceiri, P. Tomancak, A. Cardona, Fiji: an open-source platform for biological-image analysis, Nat. Methods 9 (7) (2012) 676–682.
[10] K. Kolluri, M. Demkowicz, Coarsening by network restructuring in model nanoporous gold, Acta Mater. 59 (2011) 7645–7653.
[11] P. Rios, D. Zöllner, Critical assessment 30: grain growth-Unresolved issues, Mater. Sci. Technol. 34 (6) (2018) 629–638.
[12] F. Nichols, W. Mullins, Morphological changes of a surface of revolution due to capillarity-induced surface diffusion, J. Appl. Phys. 36 (1965) 1826–1835.
[13] Y. Kwon, K. Thornton, P. Voorhees, The topology and morphology of bicontinuous interfaces during coarsening, EPL 86 (2009) 46005.
[14] J. Erlebacher, Mechanism of coarsening and bubble formation in high-Genus nanoporous metals, Phys. Rev. Lett. 106 (2011). 225504–1.
[15] K. Mangipudi, E. Epler, C. Volkert, Topology-dependent scaling laws for the stiffness and strength ofnanoporous gold, Acta Mater. 119 (2016) 115–122.
[16] D. Moldovan, D. Wolf, S. Phillpot, A. Haslam, Role of grain rotation during grain growth in a columnar microstructure by mesoscale simulation, Acta Mater. 50 (13) (2002) 3397–3414.
[17] C. Smith, Grain Shapes and Other Metallurgical Applications of Topology, in: Metals Interfaces, American Society for Metals, Cleveland, Ohio, 1952, pp. 65–113.
[18] F. Rhines, K. Craig, Mechanisms of steady-State grain growth in aluminium, Metallurgical Transactions 5 (1974) 413–425.
[19] Y. Kwon, K. Thornton, P. Voorhees, Coarsening of bicontinuous structures via nonconserved and conserved dynamics, Physical Review E 75 (2007) 021120.
[20] R. Diestel, Graph theory, Springer, New York, 2000.
[21] R. Wilson, Introduction to graph theory, 4th, Addison Wesley Longman Limited, Harlow, England, 1996.
[22] K. Mehlhorn, D. Michail, Minimum cycle bases: faster and simpler, ACM Trans. Algorithms 6 (1) (2009) 8:1–8:13.
[23] P. Gleiss, Short Cycles, Universität Wien, 2001 Ph.D. thesis.
[24] F. Harary, Graph theory, Addison Wesley, Reading, Mass., 1969.
[25] I. Bronstein, K. Semendjajew, Taschenbuch der mathematik, 23th, Harri Deutsch, Thun und Frankfurt/Main, 1987.
[26] P. Vismara, Union of all the minimum cycle bases of a graph, The Electronic Journal of Combinatorics 4 (R9) (1997) 1–15.
[27] F. Berger, P. Gritzmann, S. de Vries, Computing cyclic variants for molecular graphs, Networks 70 (2) (2017) 116–131.
[28] J. Horton, A polynomial-time algorithm to find a shortest cycle basis of a graph, SIAM Journal of Computing 16 (1987) 359–366.
[29] F. Berger, P. Gritzmann, S. de Vries, Minimum cycle bases for network graphs, Algorithmica 40 (2004) 51–62.
[30] K. Wang, J. Weissmüller, Composites of nanoporous gold and polymer, Adv. Mater. 25 (9) (2013) 1280–1284.
[31] C.-L. Park, P. Voorhees, K. Thornton, Evolution of interfacial curvatures of a bicontinuous structure generated via nonconserved dynamics, Acta Mater. 90 (2015) 182–193.
[32] C.-L. Park, J. Gibbs, P. Voorhees, K. Thornton, Coarsening of complex microstructures following spinodal decomposition, Acta Mater. 132 (2017) 13–24.
[33] D. Srolovitz, S. Safran, Capillary instabilities in thin films. i.energetics, J. Appl. Phys. 60 (1986) 247–254.
[34] H. Wong, M. Miksis, P. Voorhees, S. Davis, Universal pinch off of rods by capillarity-driven surface diffusion, Scr Mater 39 (1) (1998) 55–60.
[35] Y. Chen-Wiegart, S. Wang, Y. Chu, W. Liu, I. McNulty, P. Voorhees, D. Dunand, Structural evolution of nanoporous gold during thermal coarsening, Acta Mater. 60 (2012) 4972–4981.
[36] C. Soyarslan, S. Bargmann, M. Pradas, J. Weissmüller, 3D Stochastic bicontinuous microstructures: generation, topology and elasticity, Acta Mater. 149 (2018) 326–340.